processes

MDPI

Article

Phase Equilibria of the Ti-Nb-Mn Ternary System at 1173K, 1273K and 1373K

Chenbo Li, Hongyi Guo, Linghong Zheng, Jifeng Yang, Lideng Ye, Libin Liu and Ligang Zhang *

School of Material Science and Engineering, Central South University, Changsha 410083, China
* Correspondence: ligangzhang@csu.edu.cn; Tel.: +86-182-2949-3731 or +86-0731-8887-7732

Abstract: Phase equilibria in the Ti-Nb-Mn ternary system at 1173K, 1273K and 1373K were studied through the equilibrated alloy method by using scanning electron microscopy (SEM), electron probe microanalysis (EPMA) and X-ray diffraction (XRD) techniques. A new stable ternary phase K was confirmed and the composition was around $Ti_{50}Nb_7Mn_{43}$. A wide-range continuous solid solution phase (Ti,Nb)Mn_2 with the C14 Laves structure had been found at these temperatures due to the same phase structures of $TiMn_2$ and $NbMn_2$ phases. The solubility of Nb in $TiMn_4$, αTiMn and βTiMn intermetallic compounds was determined. Based on the experimental results and reasonable extrapolations, the isothermal sections of Ti-Nb-Mn ternary system at 1173K, 1273K and 1373K were constructed.

Keywords: Ti-Nb-Mn ternary system; phase diagram; X-ray diffraction; compounds

1. Introduction

In recent years, titanium and its alloys have been extensively used for biomedical applications, due to their high strength-to-density ratio, outstanding biocompatibility, rich microstructural features, and excellent environment and corrosion resistance [1–5]. In general, Ti-Ni alloy is widely used as bone implant material because continuing research and developmental efforts have shown its superelasticity and shape memory effect [6]. However Ni needs to be replaced by other elements due to the problems of carcinogenic and hypersensitive effects for the human body [7,8]. Ti-Nb is expected to replace Ti-Ni as a new bone implant material because of its low biological toxicity [9,10]. However, substitution of Nb also reduces the phase transformation strain, which is adverse for the application of Ti-Nb alloy in load-bearing implants [11]. Alshammari et al. found that the addition of Mn would increase the phase transformation strain of Ti-Nb alloy, and Mn, as a β -phase stable element with low cytotoxicity, was also favorable to its application in bone implants [12].

In order to optimize the microstructure and mechanical properties of a material, it is essential to have a detailed understanding of the phase equilibria and phase transformation characteristics of the alloy system [13]. Hernán et al. [14] have measured the isothermal section of Ti-Nb-Mn system in 1423K and 1473K. In order to analyze the phase relationship of this system in a larger temperature range, the phase diagrams of the Ti-Nb-Mn system at 1173K, 1273K and 1373K were investigated in this work.

In order to speculate the phase relationships of the Ti-Nb-Mn system and judge its rationality, we calculated the relevant three binary systems used CALPHAD (CALculation of PHAse Diagram) method by Pandat software, as shown in Figures 1–3. Information of binary Ti-Mn system has been extensively investigated experimentally and thermodynamic calculation [15]. As for the Ti-Mn system, Murray et al. [16] summarized a variety of experimental phase equilibria firstly, later it was optimized by Khan et al. [17] and Chen et al. [15] The assessments by Chen et al. are well consistent with the reported experiments results and thus are adopted in this work, as shown in Figure 1. There are five intermetallic compounds included-αTiMn, βTiMn, $TiMn_2$ (C14 Laves phase), $TiMn_3$ and $TiMn_4$.

check for updates

Citation: Li, C.; Guo, H.; Zheng, L.; Yang, J.; Ye, L.; Liu, L.; Zhang, L. Phase Equilibria of the Ti-Nb-Mn Ternary System at 1173K, 1273K and 1373K. *Processes* **2023**, *11*, 424. https://doi.org/10.3390/pr11020424

Academic Editor: Prashant K. Sarswat

Received: 23 December 2022
Revised: 23 January 2023
Accepted: 28 January 2023
Published: 31 January 2023

Copyright: © 2023 by the authors. Licensee MDPI, Basel, Switzerland. This article is an open access article distributed under the terms and conditions of the Creative Commons Attribution (CC BY) license (https://creativecommons.org/licenses/by/4.0/).

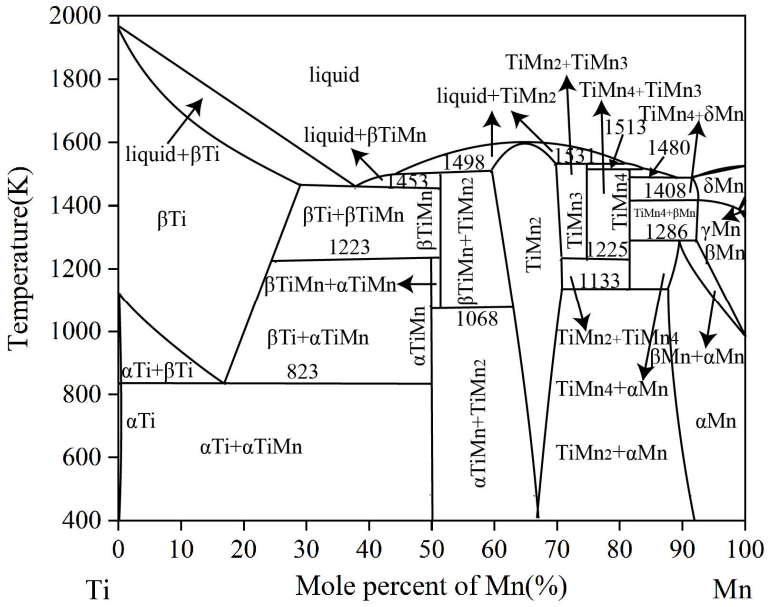

Figure 1. The calculated Ti-Mn phase diagram based on the work of Chen et al. [15].

The Nb-Mn system was thermodynamically assessed by Liu et al. [18], mainly adopting the experimental data obtained by Hellawell et al. [19], Savitskii et al. [20] and Svechnikov et al. [21] $NbMn_2$(C14 Laves phase) is the only stable intermetallic compound in Nb-Mn phase diagram. Based on the previous research work mentioned above, Liu et al. [18] reported the thermodynamic optimization of the Mn-Nb binary system, as shown in Figure 2.

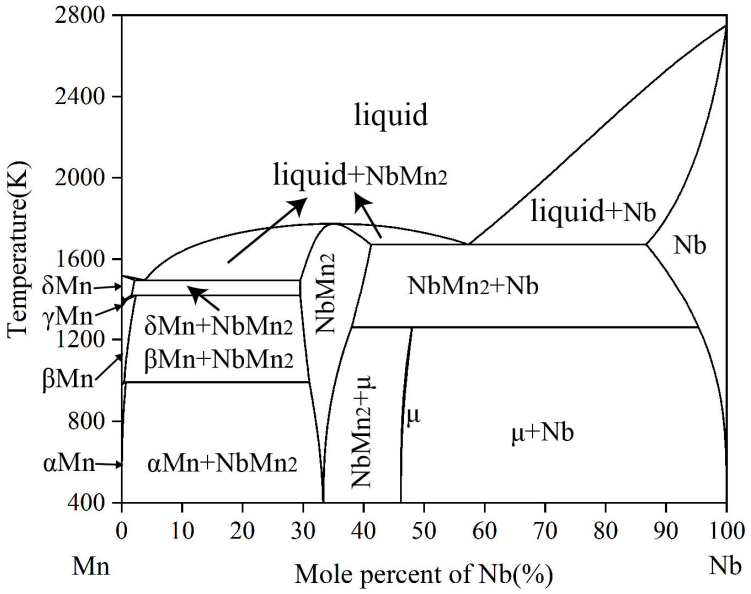

Figure 2. The calculated Mn-Nb phase diagram based on the work of Liu et al. [18].

The Ti-Nb phase diagram has been investigated by several groups [22–27]. Bellen et al. [22], Zhang et al. [26] and Matsumoto et al. [27] made a critical evaluation of this binary system. It is simple and there is no intermetallic compound and no invariant reaction, as shown in Figure 3.

So far, no information about phase relations in the Ti-Nb-Mn ternary system has been reported. The present work is an experimental study of phase relations in the Ti-Nb-Mn

system at 1173K, 1273K and 1373K through alloy samples approach. The crystallographic data of solid phases of Ti-Nb-Mn system are listed in Table 1.

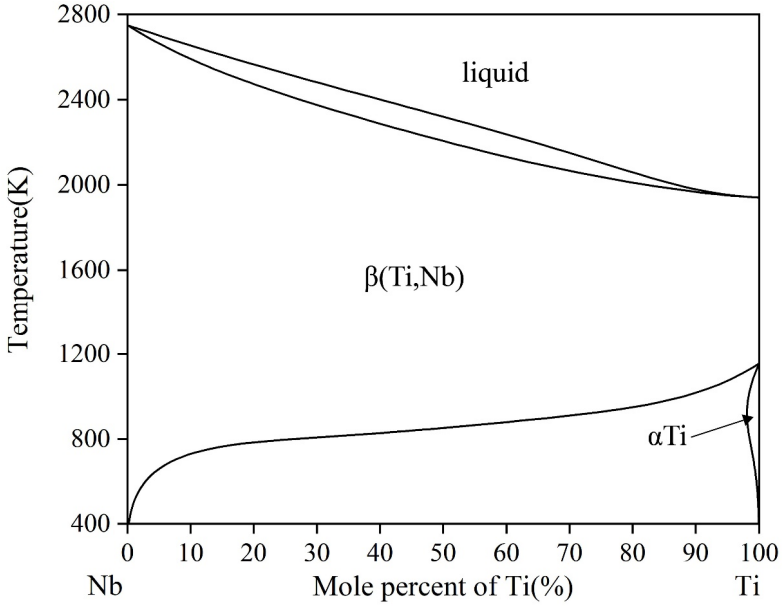

Figure 3. The calculated Ti-Nb phase diagram based on the work of Matsumoto et al. [27].

Table 1. Experimental and literature data on crystal structures and lattice parameters of the solid phases in Ti-Nb-Mn system.

Phase	Phase Prototype	Space Group	Lattice Parameters (nm)			Reference
			a	b	c	
βNb	cI2	Im-3m	0.3320	-	-	[18,28]
αTi	hP2	$P6_3/mmc$	0.2951	-	0.4684	[17]
βTi	cI2	Im-3m	0.3307	-	-	[17]
αMn	cI58	I-43m	0.8913	-	-	[17]
βMn	cP20	P4312	0.6315	-	-	[17]
γMn	cF4	Fm-3m	0.3860	-	-	[17]
αTiMn	tP30	$P4_2/mnm$	0.8731	-	0.4390	[29]
βTiMn	-	-	0.8159	-	1.2767	[29]
$TiMn_2$	hP12	$P6_3/mmc$	0.47141	-	0.78038	[17]
$TiMn_3$	oP74	Pbam	0.79081	2.58557	0.47931	[17]
$TiMn_4$	hR53	R-3	0.1007	-	0.194411	[17]
$NbMn_2$	hP12	$P6_3/mmc$	0.4802	-	0.7930	[18,28]

2. Experimental Procedure

Samples have been prepared from purity materials of 99.99% Ti, 99.99% Nb and 99.99% Mn (all in wt. %). The weight of each sample was limited to about 6 g. All the alloy samples were produced by arc-melting with a water-cooled copper plate under purified argon atmosphere, at the same time, a block of pure titanium was used as getter material placed in the arc chamber. Annealing was performed at 1173K, 1273K and 1373K for 90, 30 and 20 days respectively, alloys were taken out quickly and quenched into ice water.

Electron probe microanalysis (EPMA, JAXA-8800 R, JEOL, 15 kV, 1×10^{-8} A, Tokyo, Japan) equipped with OXFORD INCA 500 wave dispersive X-ray spectrometer (WDS) was used to detect the microstructure of equilibrated alloys and composition of each phase, including solubility. X-ray diffraction (XRD, Rigaku d-max/2550 VB, Cu K, 40 kV, 250 mA, Tokyo, Japan) was employed to analyze the crystal structure of typical alloys, with the scanning range of 10°–90° and a speed of 0.133°/s. Backscattering electron (BSE) images

of the alloy samples were acquired using a scanning electron microscope (SEM, TESCAN MIRA3 LMH, 15 kV, working distance of 15 mm, Brno, The Czech Republic).

3. Experimental Results

According to the results of EPMA-WDS data and the result of XRD patterns, the isothermal section of the Ti-Nb-Mn ternary system at 1173K has been established in Figure 4. As can be seen in Figure 4 that four intermediate compounds were detected in the Ti-Mn end at 1173K: αTiMn, βTiMn, $TiMn_2$ and $TiMn_4$. The maximum solid solubility of Nb in αTiMn and βTiMn was 1.71 at % and 3.91 at %, respectively. According to the optimization results of Ti-Mn binary system from Chen at al. [17], the composition range of αTiMn detected in this paper is very narrow, so αTiMn is treated as a linear compound in this system. At 1173K, both Ti and Nb exist in the bcc structure, so there is an area where Ti and Nb are mutually dissolved. It is worth noting that a ternary compound K-$Ti_{50}Nb_7Mn_{43}$ phase, which has never been reported before, was found in the isothermal section of the Nb-Mn-Ti ternary system at 1173K. It was mainly detected in the equilibrium alloys A7 and A10 that two three-phase equilibrium fields comprise the K-$Ti_{50}Nb_7Mn_{43}$ phase. The presence of the K-$Ti_{50}Nb_7Mn_{43}$ phase was also detected in the surrounding two-phase fields, and the composition of this ternary phase was around $Nb_7Mn_{43}Ti_{50}$. Although alloy samples of pure K-$Ti_{50}Nb_7Mn_{43}$ phase were not obtained, the existence of K-$Ti_{50}Nb_7Mn_{43}$ can be proved combining the EPMA-WDS data with the XRD results. There is only one intermediate compound at the Mn-Nb end: Mn_2Nb, and its microstructure is the same as $TiMn_2$ at the Ti-Mn end, both of which are C14 Laves phases. As shown in Table 1, because the crystal structures are completely consistent and lattice parameters are similar between βNb and βTi, the two elements Ti and Nb can be arbitrarily replaced with each other and shown as infinite solid solution β(Ti,Nb) within their composition range in Figures 4–6 [30]. Similarly, $TiMn_2$ and $NbMn_2$ can form infinite solid solution (Ti,Nb)Mn_2. At the Mn-rich end, the maximum solid solubility of Nb in $TiMn_4$ was determined to be 9.31 at.%, and the composition range of $TiMn_4$ was determined to be from 81.76 at % to 83.11 at %. Meanwhile, αMn and βMn were also detected with a certain solid solubility, but due to the strong volatility of manganese, the samples at Mn-rich end are insufficient, and its precise solid solution range cannot be obtained. Therefore, some fields are indicated by dash lines in the isothermal section.

Based on the analysis of the typical alloy samples at 1173K, the isothermal section of the Ti-Nb-Mn system at 1173K was obtained. Two three-phase equilibrium regions and ten two-phase equilibrium regions were actually detected in the isothermal section, which are: K + (Ti,Nb)Mn_2 + (βTi,Nb), K + (βTi,Nb) + βTiMn, (Ti,Nb)Mn_2 + (βTi,Nb), (βTi,Nb) + K, (βTi,Nb) + αTiMn, αTiMn + βTiMn, βTiMn + (Ti,Nb)Mn_2, K + (Ti,Nb)Mn_2, (Ti,Nb)Mn_2 + $TiMn_4$, (Ti,Nb)Mn_2 + αMn, $TiMn_4$ + αMn and αMn + βMn. Then according to the extrapolation of the three binary optimized phase diagrams and the actual determination of the phase equilibrium relationships, four undetected three-phase regions are drawn by prediction (shown by dashed lines in Figure 4), which are: βTiMn + K + (Ti,Nb)Mn_2, βTiMn + αTiMn + (βTi,Nb) and αMn + $TiMn_4$ + (Ti,Nb)Mn_2 and αMn + βMn + (Ti,Nb)Mn_2.

Based on the analysis of BSE images, EPMA-WDS data and XRD patterns, the isothermal section of the Ti-Nb-Mn system at 1273K is constructed, as presented in Figure 5. The maximum solid solubility of Nb in βTiMn and $TiMn_3$ was 3.07 at.% and 4.50 at.%, respectively. In this isothermal section, two three-phase fields and eight two-phase fields were determined by 25 equilibrium alloy samples, which are: K + (Ti,Nb)Mn_2 + (βTi,Nb), K + (βTi,Nb) + βTiMn, (Ti,Nb)Mn_2 + (βTi, Nb), (βTi,Nb) + K, K + (Ti,Nb)Mn_2, (Ti,Nb)Mn_2 + $TiMn_3$, $TiMn_3$ + $TiMn_4$, $TiMn_4$ + αMn, (Ti,Nb)Mn_2 + αMn, and (Ti,Nb)Mn_2 + βMn. Combining the three binary optimized phase diagrams, phase rules and experimental results, two undetected three-phase fields are speculated, as shown by dashed lines in Figure 5, which are: K + (Ti,Nb)Mn_2 + βTiMn, $TiMn_4$ + αMn + (Ti,Nb)Mn_2.

The isothermal section of Ti-Nb-Mn ternary system at 1373K is similar to the system at 1273K, as plotted in Figure 6. Since the isothermal section is measured at a high temperature

of 1373K, samples at the manganese-rich end are easily burned and volatilized at this temperature for a long time, by measuring only 12 equilibrium alloy samples, two three-phase equilibrium fields and four two-phase equilibrium fields are determined,which are: K + (Ti,Nb)Mn_2 + (βTi,Nb),K + (βTi,Nb) + βTiMn, (Ti,Nb)Mn_2 + (βTi,Nb), (βTi,Nb) + K, K + (Ti,Nb)Mn_2, (βTi,Nb) + βTiMn.

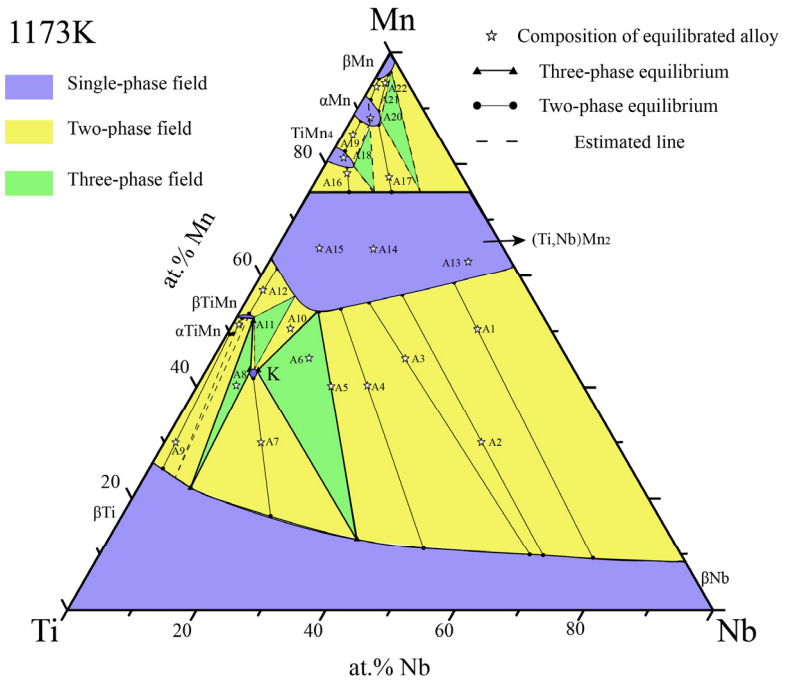

Figure 4. Isothermal section of Ti-Nb-Mn ternary system at 1173K determined in this work.

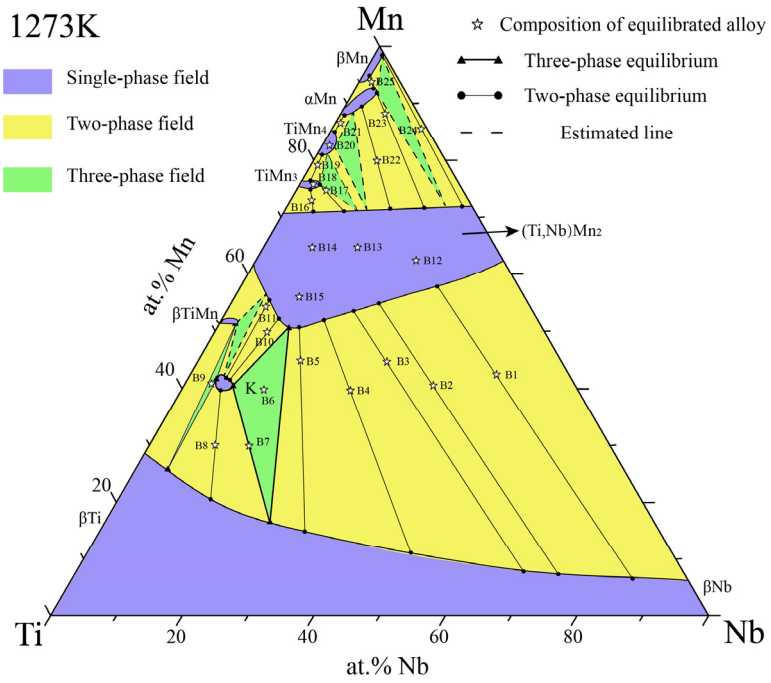

Figure 5. Isothermal section of Ti-Nb-Mn ternary system at 1273K determined in this work.

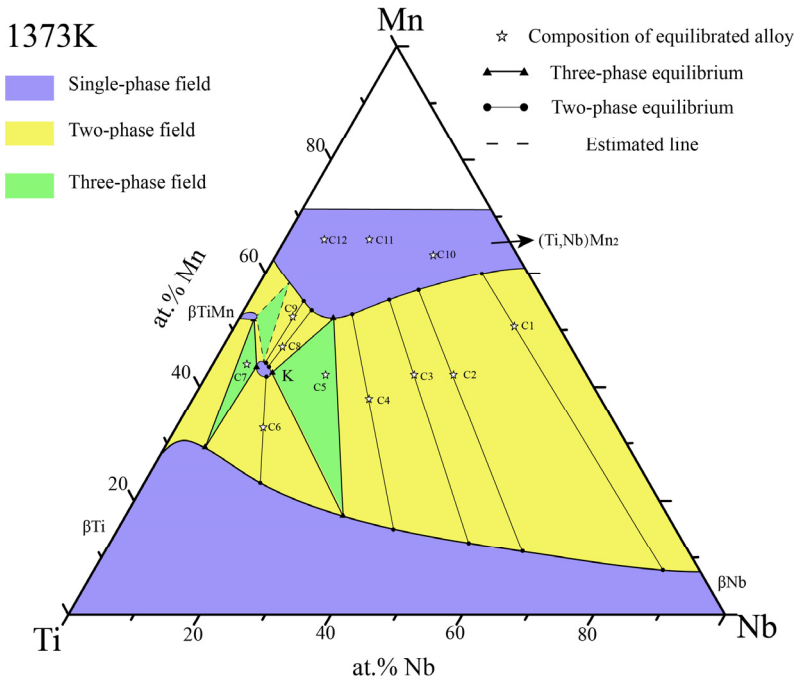

Figure 6. Isothermal section of Ti-Nb-Mn ternary system at 1373K determined in this work.

4. Discussion

To determine the phase relationships of the Ti-Nb-Mn ternary system at 1173K, 1273K and 1373K, a series of specimens were prepared. Tables 2–4 list the nominal composition of the ternary alloy samples respectively. All phases formed in the specimens, together with the chemical composition of the phases are included in Tables 2–4.

Table 2. Constituent phases and compositions in the annealed Ti-Nb-Mn alloys at 1173K for 90 days.

Alloys No.	Nominal Composition (at %)			Experimental Results (at %)			Phase Determination
	Ti	Nb	Mn	Ti	Nb	Mn	
A1	10	50	40	13.91	76.62	9.47	(βTi,Nb)
				10.75	29.81	59.44	(Ti,Nb)Mn_2
A2	20	50	30	21.78	68.53	9.69	(βTi,Nb)
				19.9	23.21	56.89	(Ti,Nb)Mn_2
A3	25	30	45	23.61	66.7	9.69	(βTi,Nb)
				26.44	18.38	55.18	(Ti,Nb)Mn_2
A4	35	25	40	40.37	48.39	11.24	(βTi,Nb)
				30.66	14.91	54.43	(Ti,Nb)Mn_2
A5	40	20	40	48.18	38.97	12.85	(βTi,Nb)
				34.77	11.91	53.32	(Ti,Nb)Mn_2
A6	40	15	45	48.68	38.57	12.75	(βTi,Nb)
				34.27	11.91	53.82	(Ti,Nb)Mn_2
				49.24	7.92	42.84	K
A7	55	15	30	60.07	22.79	17.14	(βTi,Nb)
				50.89	8.37	40.74	K
A8	55	5	40	70.13	8.04	21.83	(βTi,Nb)
				50.88	6.89	42.23	K
				45.63	3.45	50.92	βTiMn
A9	68	2	30	49.39	0.68	49.93	αTiMn
				72.53	2.26	25.21	(βTi,Nb)
A10	42	9	49	48.99	8.23	42.78	K
				36.94	9.41	53.65	(Ti,Nb)Mn_2

Table 2. *Cont.*

Alloys No.	Nominal Composition (at %)			Experimental Results (at %)			Phase Determination
	Ti	Nb	Mn	Ti	Nb	Mn	
A11	47	4	49	45.69	3.01	51.3	βTiMn
				49.98	7.36	42.66	K
A12	40	2	58	36.67	2.18	61.15	$(Ti,Nb)Mn_2$
				44.99	1.9	53.11	(βTi,Nb)
A13	7	30	63	6.79	30.27	62.94	$(Ti,Nb)Mn_2$
A14	20	15	65	19.91	15.11	64.98	$(Ti,Nb)Mn_2$
A15	30	5	65	28.42	6.93	64.65	$(Ti,Nb)Mn_2$
A16	17.5	4	78.5	17.16	3.57	79.27	$TiMn_4$
				19.06	5.7	75.24	$(Ti,Nb)Mn_2$
A17	10	10	80	7.02	2.95	90.03	αMn
				12.78	15.65	71.57	$(Ti,Nb)Mn_2$
A18	15	2	83	17.96	2.39	79.65	$TiMn_4$
A19	14	1	85	14.44	1.51	84.05	$TiMn_4$
				10.73	1.32	87.95	αMn
A20	9	1	90	8.91	2.06	89.03	αMn
A21	5	1	94	7.04	0.72	92.24	αMn
				3.39	0.97	95.64	βMn
A22	3	2	95	6.91	2.16	90.93	αMn
				2.1	2.03	95.87	βMn

4.1. Phase Equilibria at 1173K

Twenty-two alloy samples were prepared in order to determine the isothermal section and phase relationship of the Ti-Nb-Mn ternary system at 1173K. The constituent phases of each alloy sample were listed in Table 2. In this table, nominal composition was set before synthesizing alloy and the content of each element in phase is measured by WDS.

As shown in Figure 7a, EPMA analysis indicates that it contains a two-phase region. With the help of XRD method (Figure 7b), these two phases were confirmed as (βTi,Nb) (white base phase) and $TiMn_2$ (gray phase). Considering $TiMn_2$ and $NbMn_2$ phases have the same C14 crystal structure, they can form a wide-range continuous solid solution phase $(Ti,Nb)Mn_2$. A similar situation occurs in another system [18], they found that the $(Zr,Ti)Mn_2$ phase maintained the C14 structure with the change of the composition ratio of Zr and Ti. In order to confirm it, samples of A12, A13 and A14 alloys were prepared.

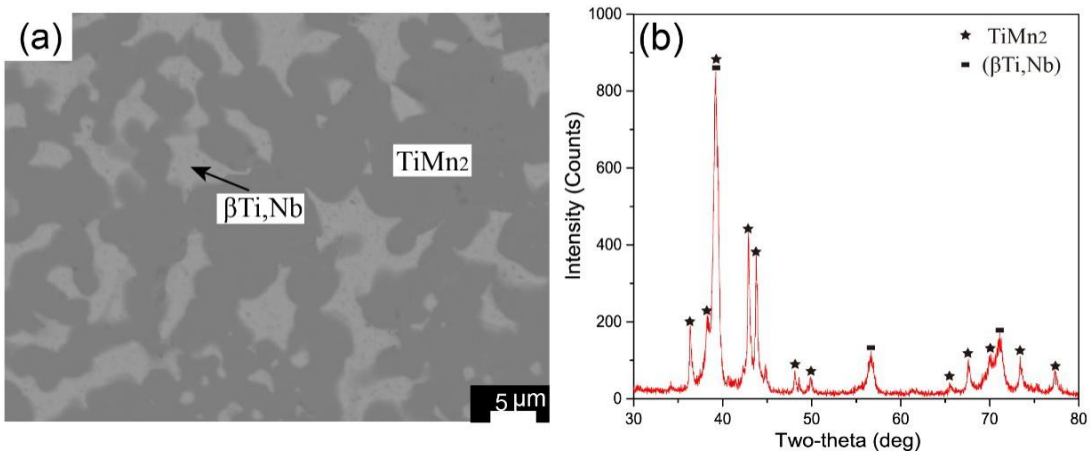

Figure 7. Alloy A2 annealed at 1173K for 90 days: (**a**) back-scattered electron (BSE) images, (**b**) XRD patterns.

The microstructure of A7 and A10 are shown in Figures 8a and 9a. Using SEM-EDS and EPMA, we found the phase composition of the A7 alloy sample is (βTi,Nb) (white base phase) and K-$Ti_{50}Nb_7Mn_{43}$ phase (dark gray phase), while the A10 alloy comprises

(Ti,Nb)Mn_2 (light-colored base phase) and K-$Ti_{50}Nb_7Mn_{43}$ phase (dark phase). According to Figures 8a and 9a, the equilibrium alloys A7 and A10 are both composed by two different phases, including an unknown ternary compound whose microstructure and XRD result have never been reported. This ternary compound is referred to herein as K-$Ti_{50}Nb_7Mn_{43}$ phase. Since there is no corresponding PDF card, the XRD results of the two equilibrium alloys containing the K-$Ti_{50}Nb_7Mn_{43}$ phase are put together for comparative analysis, as presented in Figures 8b and 9b. In Figures 8b and 9b, after the characteristic peaks of the other phases were matched, the remaining diffraction peaks can be well matched with the obtained unknown ternary phase K-$Ti_{50}Nb_7Mn_{43}$. Thus, the existence of K-$Ti_{50}Nb_7Mn_{43}$ can be determined. The composition of this ternary phase was around $Ti_{50}Nb_7Mn_{43}$ from the results of EPMA.

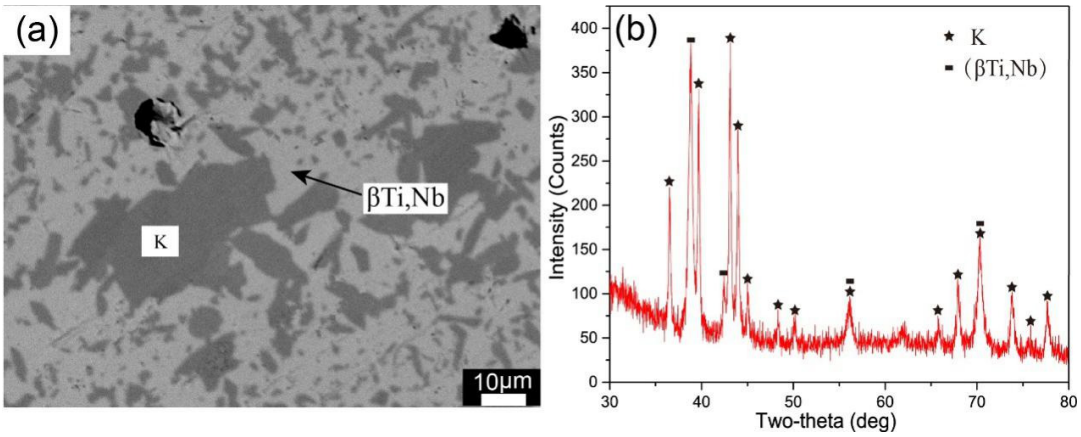

Figure 8. Alloy A7 annealed at1173K for 90 days: (**a**) back-scattered electron (BSE) images and (**b**) XRD patterns.

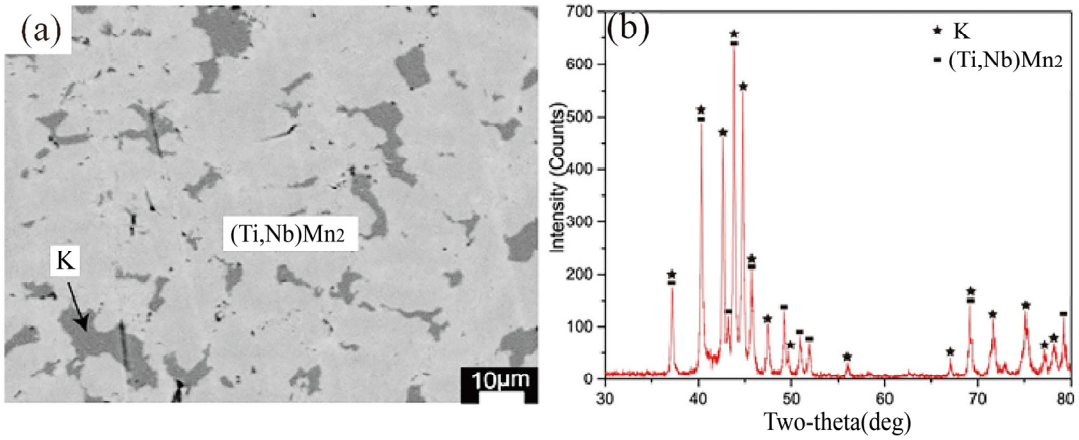

Figure 9. Alloy A10 annealed at1173K for 90 days: (**a**) back-scattered electron (BSE) images and (**b**) XRD patterns.

Three different phases can be observed in Figure 10a: βTiMn (white phase), K-$Ti_{50}Nb_7Mn_{43}$ phase (light gray phase) and (βTi,Nb) (dark gray phase). Although the contrast between the K-$Ti_{50}Nb_7Mn_{43}$ phase and (βTi,Nb) doesn't have a significant difference, there is a boundary between these two phases and the XRD results of them are completely different. Based on this, it can be judged that the alloy A8 is located in the three-phase equilibrium field: K + βTiMn + (βTi,Nb), which is also consistent with the XRD results from Figure 10b.

Based on the microstructure results and XRD pattern analyses of Figures 11–13, it can be judged that the alloy A12, A16 and A17 are composed of two phases after reaching

equilibrium at 1173K. The A12 alloy is located in the two-phase equilibrium field: βTiMn + (Ti,Nb)Mn_2; The dark gray base phase in the equilibrium alloy A16 is (Ti,Nb)Mn_2, and the white globular phase attached to the base phase is $TiMn_4$; A17 contains two phases: (Ti,Nb)Mn_2 (gray phase) and αMn (white dendritic phase).

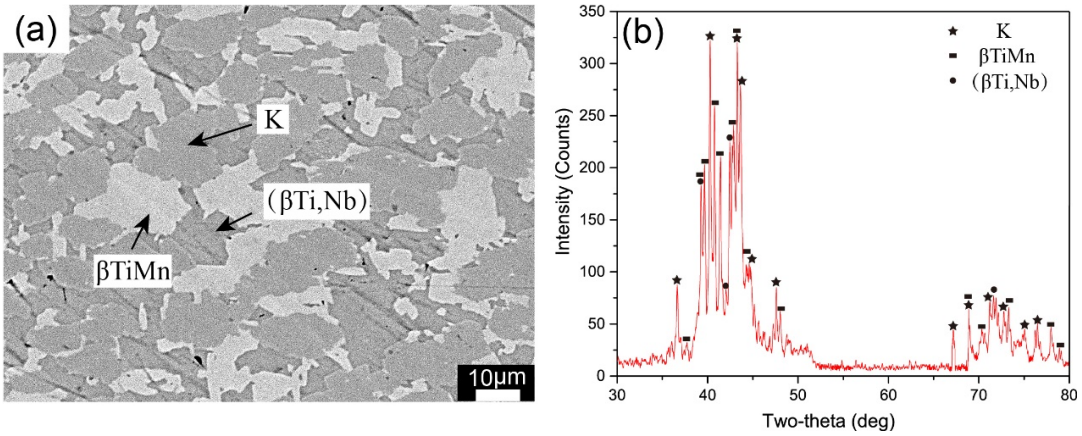

Figure 10. Alloy A8 annealed at 1173K for 90 days: (**a**) back-scattered electron (BSE) images, (**b**) XRD patterns.

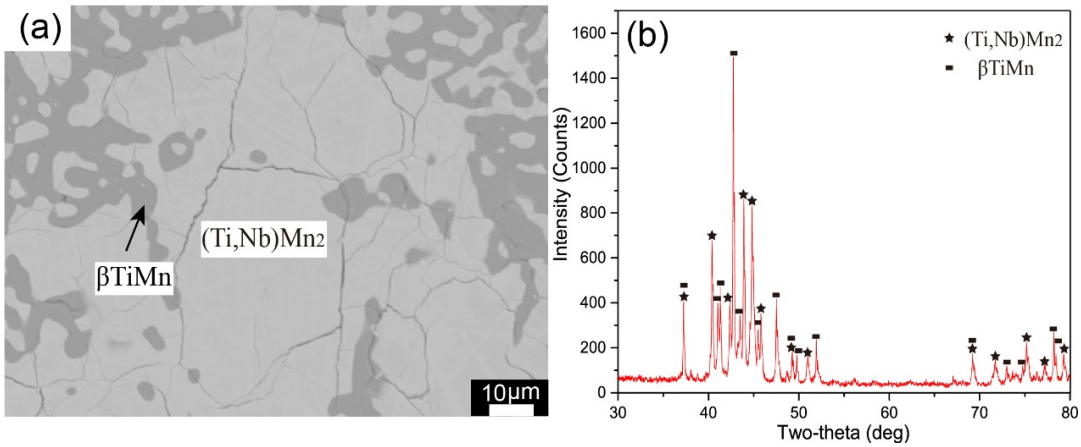

Figure 11. Alloy A12 annealed at 1173K for 90 days: (**a**) back-scattered electron (BSE) images, (**b**) XRD patterns.

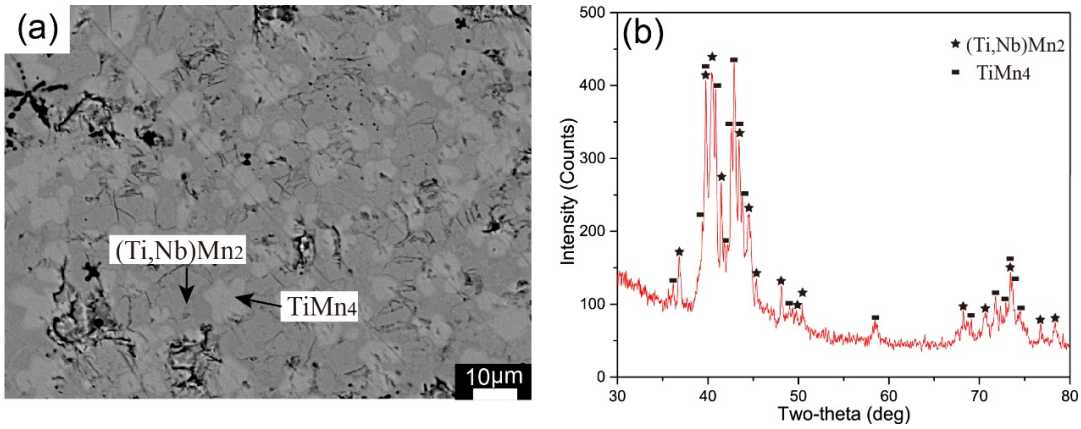

Figure 12. Alloy A16 annealed at 1173K for 90 days: (**a**) back-scattered electron (BSE) images, (**b**) XRD patterns.

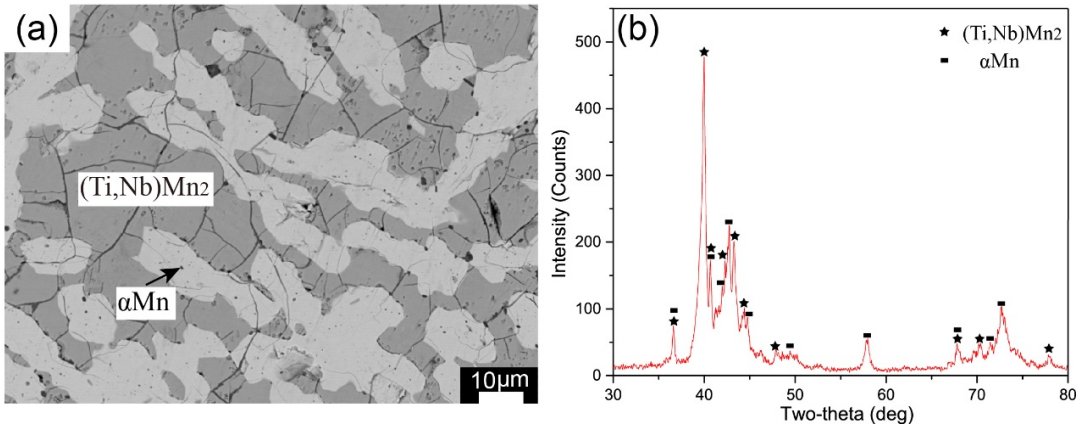

Figure 13. Alloy A17 annealed at 1173K for 90 days: (**a**) back-scattered electron (BSE) images, (**b**) XRD patterns.

4.2. Phase Equilibria at 1273K

Twenty-five alloy samples were prepared in order to determine the isothermal section and phase relationship of the Ti-Nb-Mn ternary system at 1273K for 30 days. The constituent phases of each alloy sample were listed in Table 3.

Table 3. Constituent phases and compositions in the annealed Ti-Nb-Mn alloys at 1273K for 30 days.

Alloys No.	Nominal Composition (at %)			Experimental Results (at %)			Phase Determination
	Ti	Nb	Mn	Ti	Nb	Mn	
B1	11	47	42	8.56	84.95	6.49	(βTi,Nb)
				12.6	29.3	58.1	$(Ti,Nb)Mn_2$
B2	22	38	40	19.2	73.13	7.67	(βTi,Nb)
				22.5	22.57	54.93	$(Ti,Nb)Mn_2$
B3	27	27	46	23.99	67.7	8.31	(βTi,Nb)
				26.73	19.31	53.96	$(Ti,Nb)Mn_2$
B4	35	27	38	40.37	48.39	11.24	(βTi,Nb)
				31.66	15.62	52.72	$(Ti,Nb)Mn_2$
B5	40	15	45	53.86	29.12	17.02	(βTi,Nb)
				36.37	12.86	50.77	$(Ti,Nb)Mn_2$
B6	47	12	41	58.19	24.83	16.98	(βTi,Nb)
				38.69	11.25	50.06	$(Ti,Nb)Mn_2$
				51.96	7.4	40.64	K
B7	54	16	30	58.07	24.45	17.48	(βTi,Nb)
				37.97	11.45	50.58	$(Ti,Nb)Mn_2$
				51.88	7.34	40.78	K
B8	59	10	31	65.8	13.78	20.42	(βTi,Nb)
				54.84	5.9	39.26	K
B9	56	4	40	69.01	4.8	26.19	(βTi,Nb)
				53.13	4.21	42.66	K
				46.89	2.22	50.89	βTiMn
B10	42	8	50	39.24	8.24	52.52	$(Ti,Nb)Mn_2$
				52.38	6.01	41.61	K
B11	42	6	52	39.24	5.37	55.39	$(Ti,Nb)Mn_2$
				52.37	5.42	42.21	K
B12	14	24	62	51.91	5.42	42.67	$(Ti,Nb)Mn_2$
B13	20	15	65	20.05	14.78	65.17	$(Ti,Nb)Mn_2$
B14	27	8	65	26.7	8.11	65.19	$(Ti,Nb)Mn_2$
B15	34	8	58	35.12	8.37	56.51	$(Ti,Nb)Mn_2$
B16	23	4	73	24.28	4.56	71.16	$(Ti,Nb)Mn_2$
				22.71	2.54	74.75	$TiMn_3$

Table 3. *Cont.*

Alloys No.	Nominal Composition (at %)			Experimental Results (at %)			Phase Determination
	Ti	Nb	Mn	Ti	Nb	Mn	
B17	20	5	75	19.65	8.66	71.69	(Ti,Nb)Mn_2
				21.38	3.74	74.88	$TiMn_3$
B18	22	2	76	22.45	1.65	75.9	$TiMn_3$
B19	20	1	79	21.73	1.12	77.15	$TiMn_3$
				18.33	0.95	80.72	$TiMn_4$
B20	15	2	83	17.63	1.24	81.13	$TiMn_4$
B21	12	1	87	11.73	0.32	87.95	αMn
				14.44	0.51	85.05	$TiMn_4$
B22	10	10	80	8.01	2.45	89.54	αMn
				12.58	15.62	71.8	(Ti,Nb)Mn_2
B23	5	7	88	4.29	3.98	91.73	αMn
				7.42	20.46	72.12	(Ti,Nb)Mn_2
B24	1	12	87	0.24	1.79	97.97	βMn
				1.27	25.67	73.06	(Ti,Nb)Mn_2
B25	4	2	94	4.23	2.93	92.84	αMn
				3.94	1.56	94.5	βMn

According to the microstructure results in Figures 14a and 15a, the alloy B6 consists of three phases: (βTi,Nb) (white base phase), (Ti,Nb)Mn_2 (light gray phase) and the K phase (dark gray phase); the alloy B9 is composed of βTiMn (white phase), the K-$Ti_{50}Nb_7Mn_{43}$ phase (gray striped phase) and (βTi,Nb) (black phase). In Figures 14b and 15b, after the characteristic peaks of the other two phases were matched, the remaining diffraction peaks can be well matched with the previously obtained unknown ternary phase K-$Ti_{50}Nb_7Mn_{43}$. Thus, the existence of K-$Ti_{50}Nb_7Mn_{43}$ can be determined.

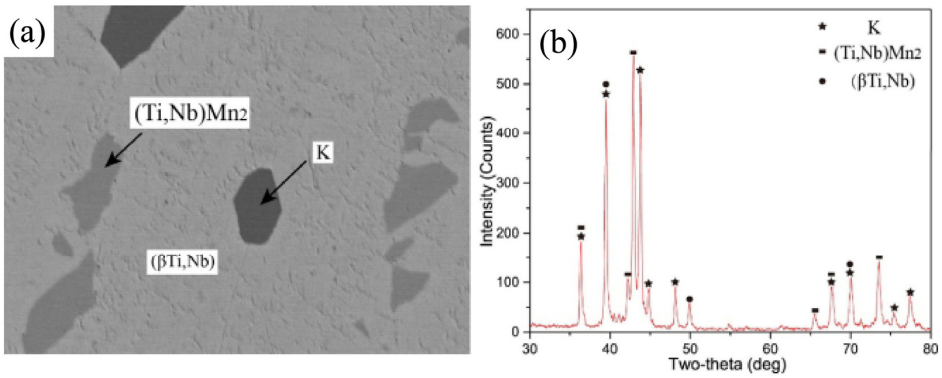

Figure 14. Alloy B6 annealed at 1273K for 60 days: (**a**) BSE images, (**b**) XRD patterns.

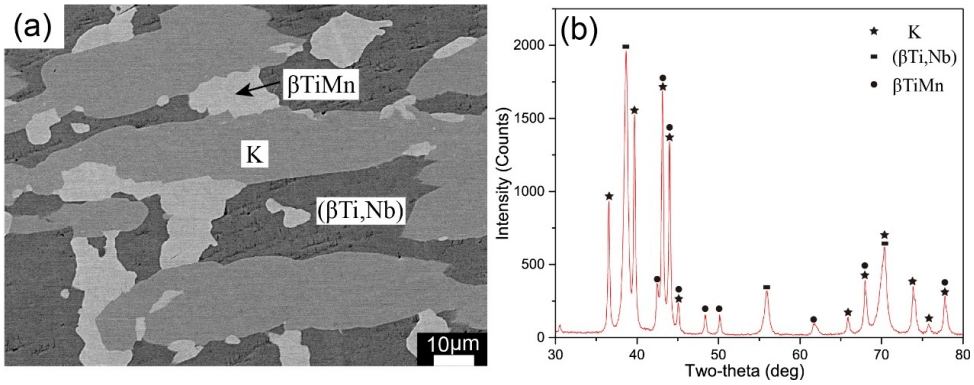

Figure 15. Alloy B9 annealed at 1273K for 60 days: (**a**) BSE images, (**b**) XRD patterns.

As shown in Figure 16a, there are two distinct phases in the alloy B1. Based on the XRD pattern analysis in Figure 16b, the alloy should be located in the two-phase field: (Ti,Nb)Mn_2 + (βTi,Nb). Figure 17a,b are BSE images of alloys B2 and B4 also located in the two-phase field. It can be clearly observed that the phase (Ti,Nb)Mn_2 continues to grow with increasing Ti content.

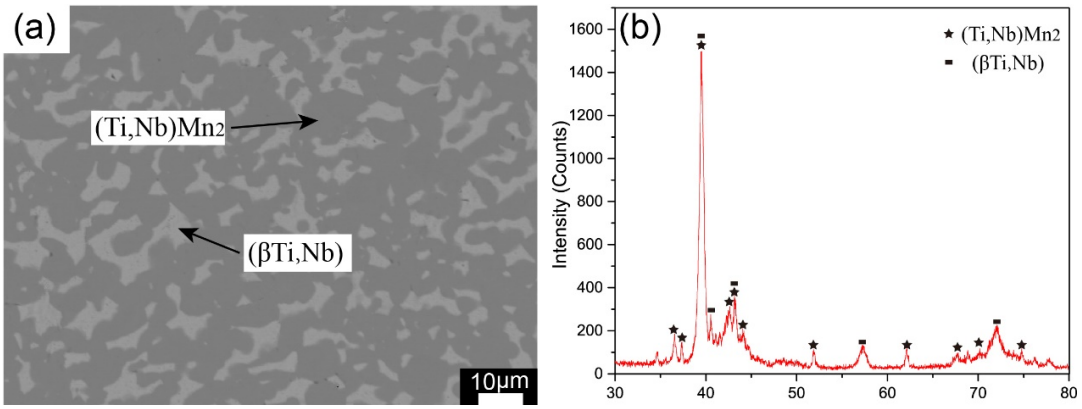

Figure 16. Alloy B1 annealed at 1273K for 60 days: (**a**) BSE images, (**b**) XRD patterns.

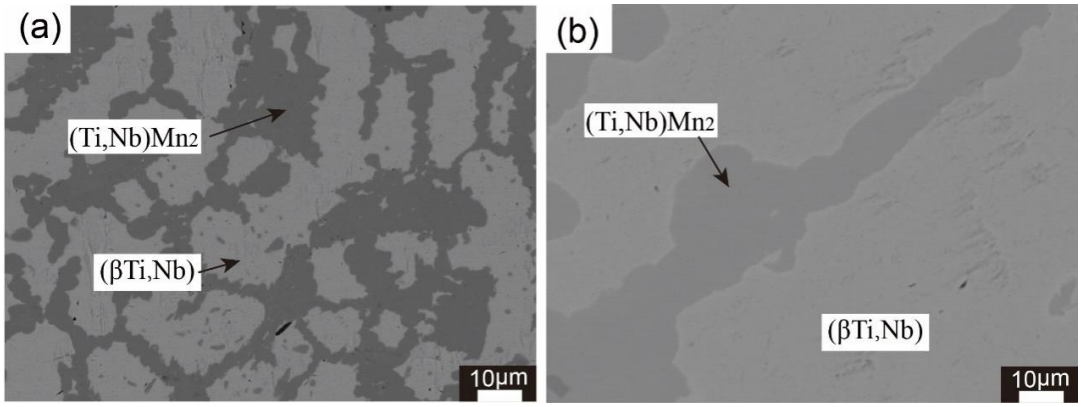

Figure 17. BSE images of alloys annealed at 1273K for 60 days: (**a**) B2, (**b**) B4.

Figures 18–22 respectively show the EPMA micrographs and XRD results of alloy B8, B10, B16, B19 and B25, which featured 5 two-phase equilibriums: K + (βTi,Nb), K + (Ti,Nb)Mn_2, $TiMn_3$ + $TiMn_2$, $TiMn_3$ + $TiMn_4$ and αMn + βMn.

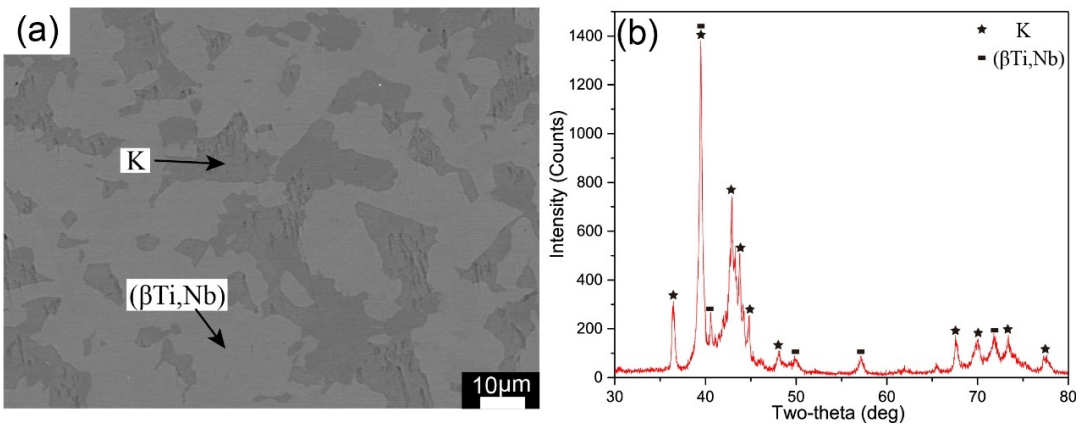

Figure 18. Alloy B8 annealed at 1273K for 60 days: (**a**) BSE images, (**b**) XRD patterns.

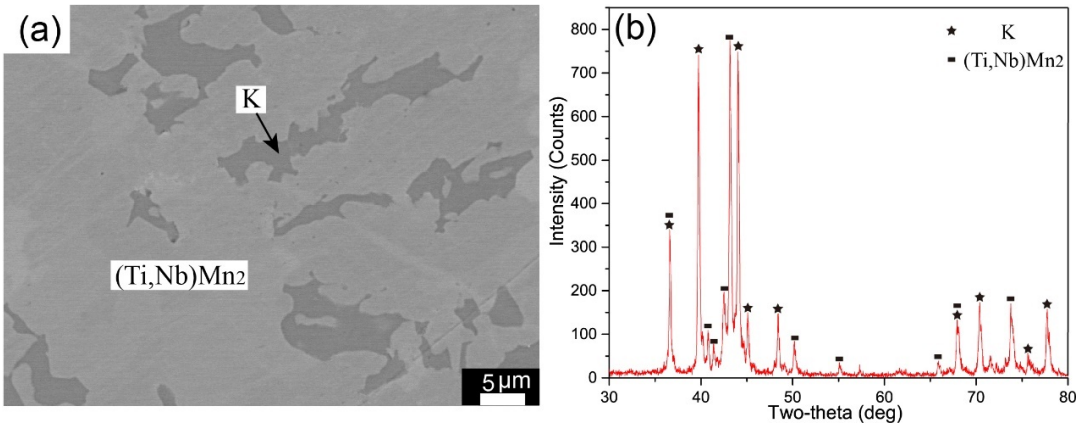

Figure 19. Alloy B10 annealed at 1273K for 60 days: (**a**) BSE images, (**b**) XRD patterns.

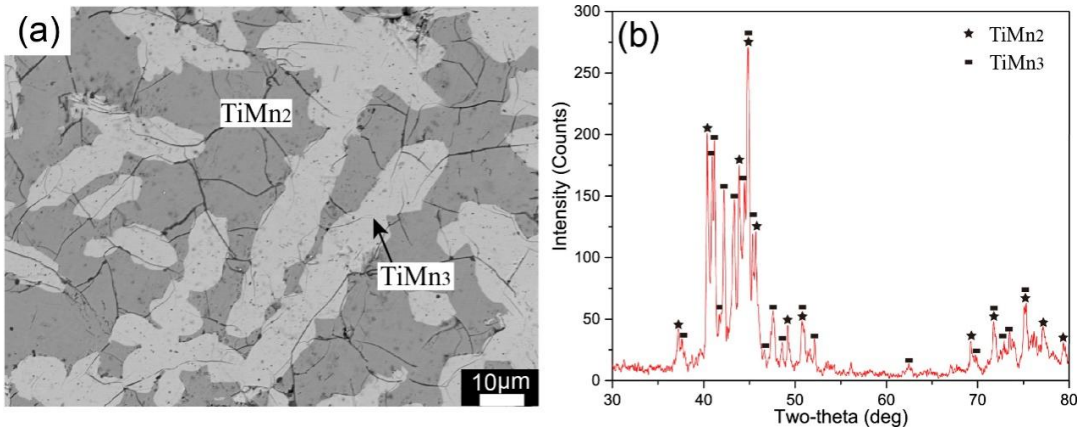

Figure 20. Alloy B16 annealed at 1273K for 60 days: (**a**) BSE images, (**b**) XRD patterns.

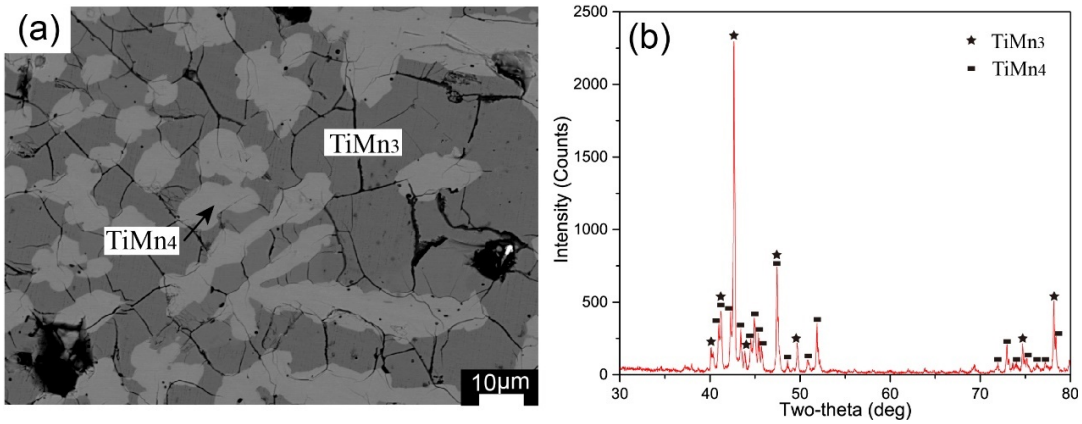

Figure 21. Alloy B19 annealed at 1273K for 60 days: (**a**) BSE images, (**b**) XRD patterns.

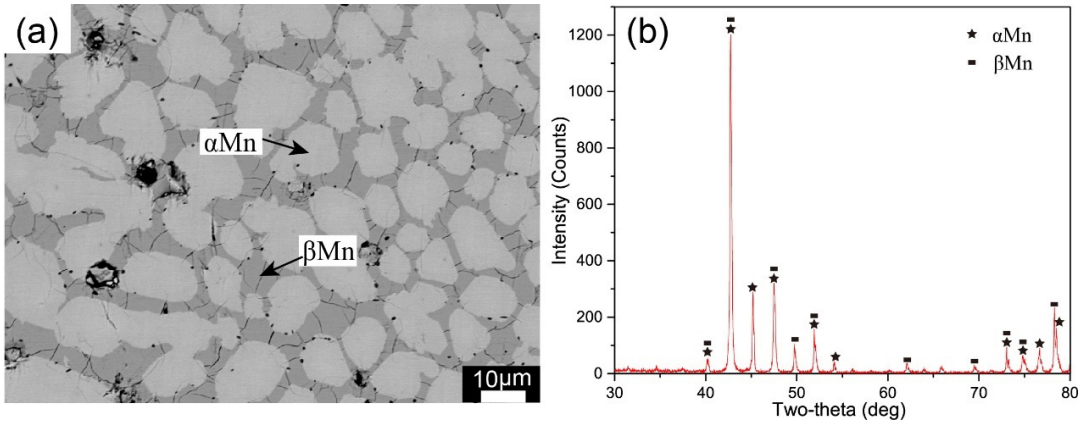

Figure 22. Alloy B25 annealed at 1273K for 60 days: (**a**) BSE images, (**b**) XRD patterns.

It can be observed in Figure 23 that the alloy B21, B22 and B24 are respectively in 3 two-phase equilibrium fields: $TiMn_4$ + αMn, (Ti,Nb)Mn_2 + αMn and (Ti,Nb)Mn_2 + βMn; the alloy B14 is in the solid solution field: (Ti,Nb)Mn_2.

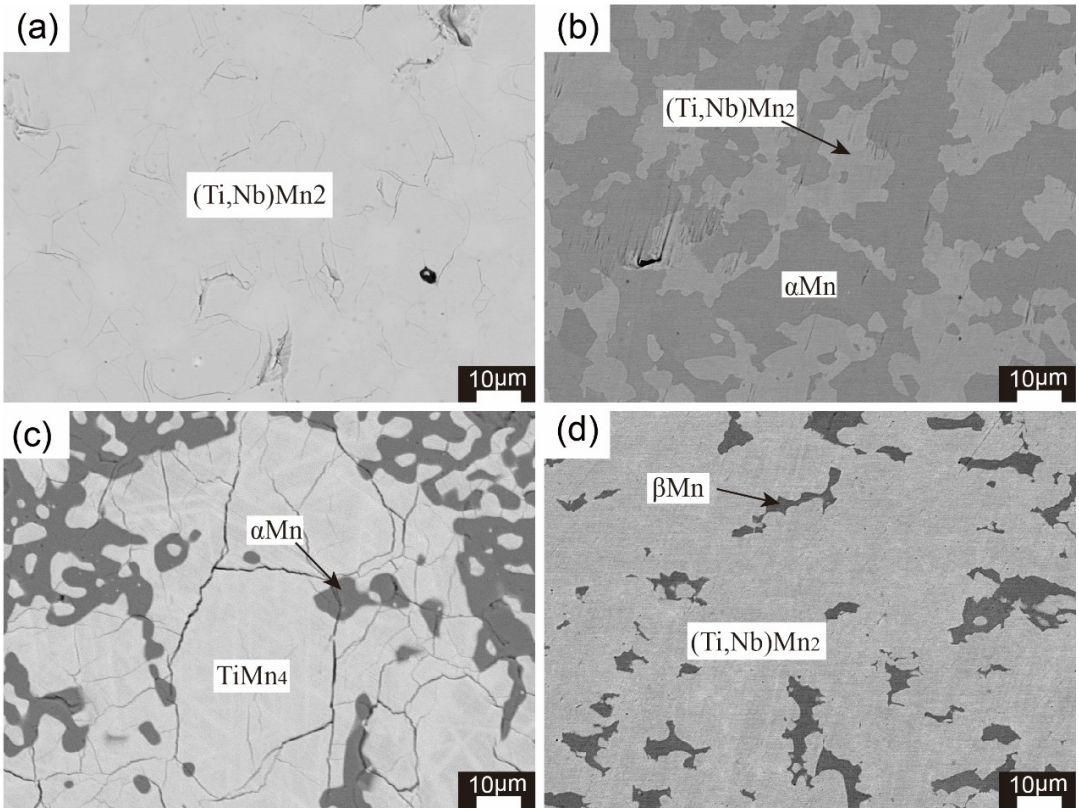

Figure 23. BSE images of alloys annealed at 1273K for 60 days: (**a**) B14, (**b**) B22, (**c**) B21, (**d**) B24.

4.3. Phase Equilibria at 1373K

12 alloy samples were prepared in order to determine the isothermal section and phase relationship of the Ti-Nb-Mn ternary system at 1373K for 20 days. The constituent phases of each alloy sample were listed in Table 4.

The microstructure of the equilibrium alloy C5 after annealing is shown in Figure 24a. Based on the EPMA result, (βTi,Nb) (white base phase), (Ti,Nb)Mn_2 (light gray phase) and the K-$Ti_{50}Nb_7Mn_{43}$ phase (dark gray phase) with the unknown crystal structure can be determined. In Figure 24b, After calibration of (βTi,Nb) and (Ti,Nb)Mn_2 by the existing

PDF card, the remaining characteristic peaks can correspond with the peaks of the previous K-$Ti_{50}Nb_7Mn_{43}$ phase. It is determined the alloy C5 is located in the three-phase field: (βTi,Nb) + (Ti,Nb)Mn_2 + K. And Figure 25a shows the three-phase microstructure of K + (βTi,Nb) + βTiMn for the equilibrium alloy C7 after anneal at 1373K.

Table 4. Constituent phases and compositions in the annealed Ti-Nb-Mn alloys at 1373 K for 20 days.

Alloys No.	Nominal Composition (at %)			Experimental Results (at %)			Phase Determination
	Ti	Nb	Mn	Ti	Nb	Mn	
C1	6	43	51	5.63	86.53	7.84	(βTi,Nb)
				6.61	33.19	60.2	(Ti,Nb)Mn_2
C2	20	38	42	24.98	63.99	11.03	(βTi,Nb)
				18.05	25.07	56.88	(Ti,Nb)Mn_2
C3	27	33	40	32.75	54.5	12.75	(βTi,Nb)
				23.64	21.22	55.14	(Ti,Nb)Mn_2
C4	36	28	36	42.99	41.73	15.28	(βTi,Nb)
				30.31	17.07	52.62	(Ti,Nb)Mn_2
C5	40	18	42	47.57	9.54	42.89	K
				49.84	33.02	17.14	(βTi,Nb)
				32.98	14.07	52.95	(Ti,Nb)Mn_2
C6	54	13	33	49.78	9.19	41.03	K
				58.94	17.35	23.71	(βTi,Nb)
C7	53	5	42	46.14	2.3	51.56	βTiMn
				64.34	5.76	29.9	(βTi,Nb)
				49.67	6.75	43.58	K
C8	44	9	47	36.22	8.1	55.68	(Ti,Nb)Mn_2
				47.58	7.64	44.78	K
C9	40	8	52	36.23	10.34	53.43	(Ti,Nb)Mn_2
				47.35	8.8	43.85	K
C10	13	23	64	13.3	23.31	63.39	(Ti,Nb)Mn_2
C11	22	13	65	21.12	13.64	65.24	(Ti,Nb)Mn_2
C12	30	7	63	28.72	6.97	64.31	(Ti,Nb)Mn_2

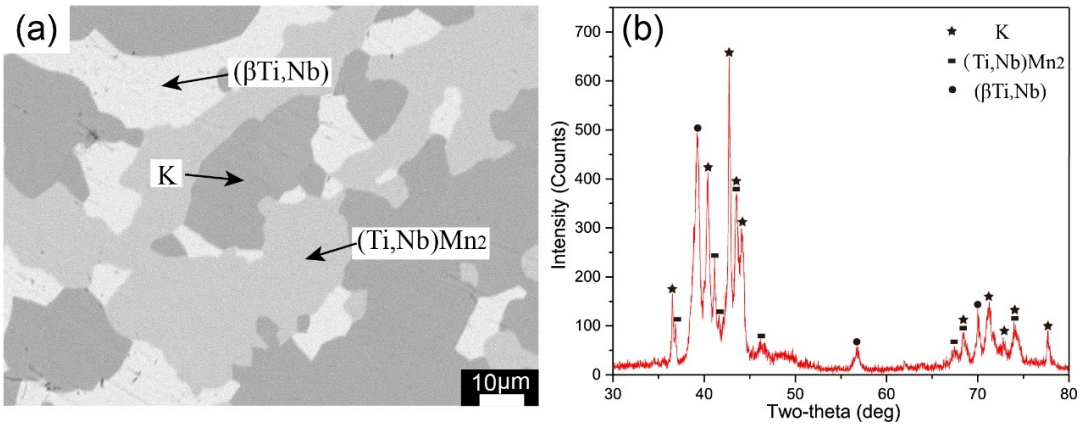

Figure 24. Alloy C5 annealed at 1373K for 40 days: (**a**) BSE images, (**b**) XRD patterns.

Figure 26a shows the microstructure of the equilibrium alloy C3 annealed at 1100 °C for 40 days, which contains (βTi,Nb) (white base phase) and (Ti,Nb)Mn_2 (gray phase) based on the EPMA result. Figure 27a shows the two-phase K + (βTi,Nb) microstructure for the equilibrium alloy C6 that agrees with the XRD result presented in Figure 27b.

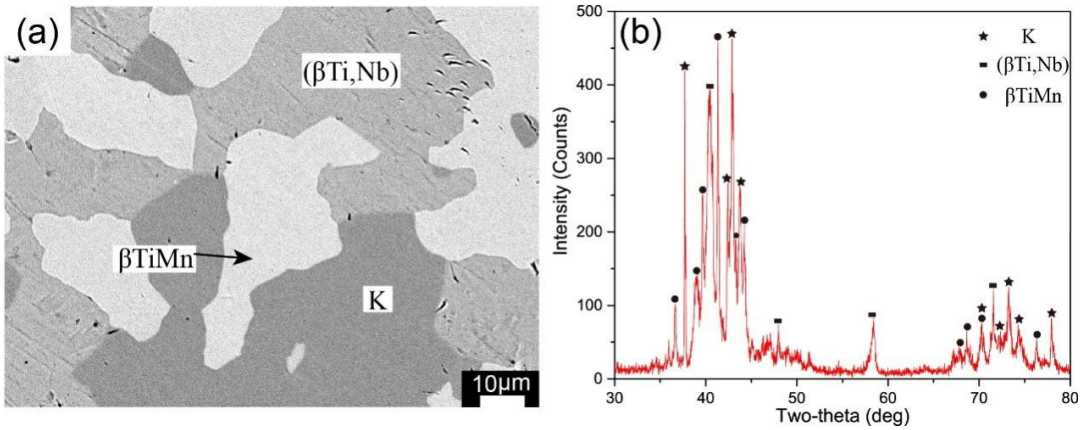

Figure 25. Alloy C7 annealed at 1373K for 40 days: (**a**) BSE images, (**b**) XRD patterns.

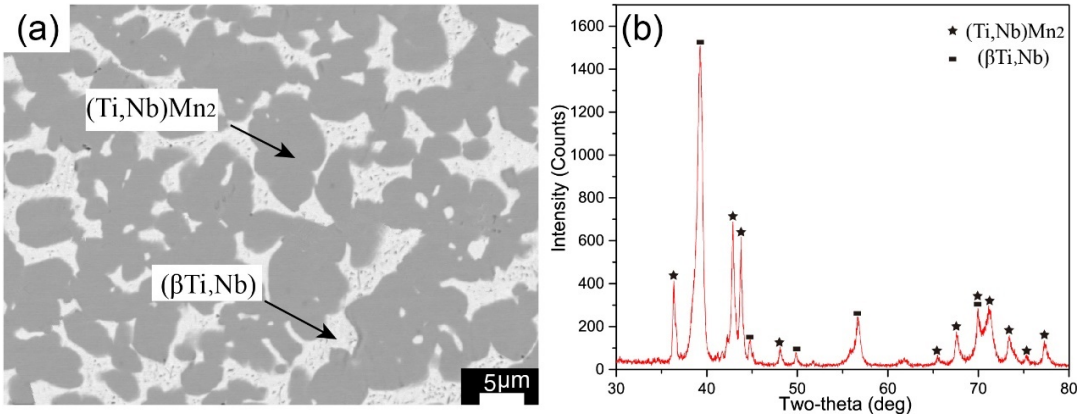

Figure 26. Alloy C3 annealed at 1373K for 40 days: (**a**) BSE images, (**b**) XRD patterns.

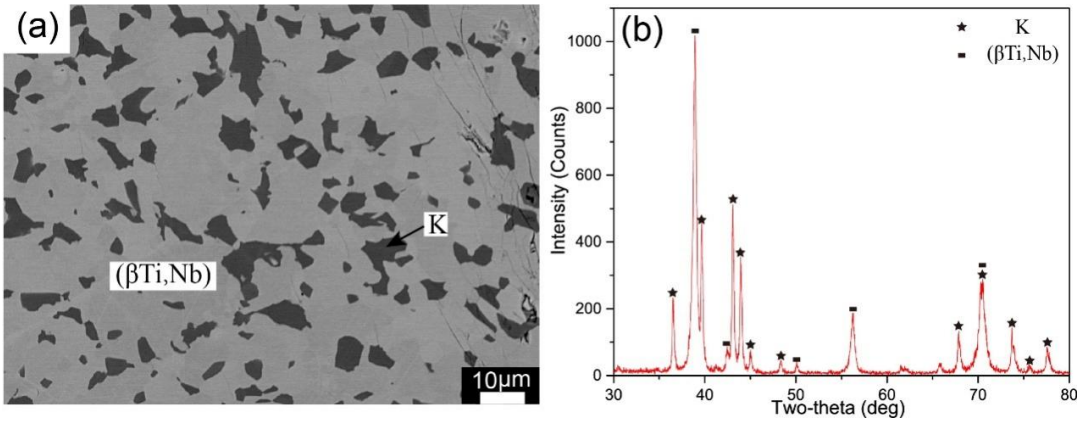

Figure 27. Alloy C6 annealed at 1373K for 40 days: (**a**) BSE images, (**b**) XRD patterns.

5. Conclusions

The isothermal section of Ti-Nb-Mn system at 1173K, 1273K and 1373K were determined by equilibrium alloy method combined with EPMA-WDS and XRD. The results are summarized as follows: (1) A new ternary compound K-$Ti_{50}Nb_7Mn_{43}$ phase was detected at 1173K, 1273K and 1373K. And a continuous solid solution phase (Ti,Nb)Mn_2 was found at these temperatures in this ternary system. (2) Three three-phase equilibrium fields and ten two-phase equilibrium fields were detected in the isothermal section at 1173K, the

experimentally determined maximum solid solubility of Nb in αTiMn and βTiMn were 1.71 at % and 3.91 at %, respectively; the maximum solid solubility of Nb in $TiMn_4$ was 9.31 at %. (3) Two three-phase equilibrium fields and eight two-phase equilibrium fields were detected in the isothermal section at 1273K. The maximum solid solubility of Nb in βTiMn was 3.07 at % and in $TiMn_3$ was 4.50 at %; (4) For the isothermal section of 1373K, the maximum solid solubility of Nb in βTiMn was measured to be 5. 68 at %.

Author Contributions: Conceptualization, L.Z. (Ligang Zhang) and C.L.; Methodology, H.G.; Software, L.Z. (Linghong Zheng); Validation, J.Y.; Formal analysis, C.L. and L.Y.; Investigation, C.L. and H.G.; Resources, J.Y. and L.Y.; Data curation, L.Y.; Writing—original draft preparation, C.L.; Writing—review and editing, C.L.; Visualization, L.L.; Supervision, L.Z. (Ligang Zhang); Project administration, L.Z. (Ligang Zhang); Funding acquisition, L.Z. (Ligang Zhang) All authors have read and agreed to the published version of the manuscript.

Funding: The work was financially supported by National MCF Energy R&D Program of China (No. 2018YFE0306100), National Natural Science Foundation of China (No. 51871248), and Natural Science Foundation of Hunan Province, China (No. 2020JJ4739).

Data Availability Statement: Not applicable.

Conflicts of Interest: The authors declare no conflict of interest.

References

1. Baltatu, M.S.; Spataru, M.C.; Verestiuc, L.; Balan, V.; Solcan, C.; Sandu, A.V.; Geanta, V.; Voiculescu, I.; Vizureanu, P. Design, Synthesis, and Preliminary Evaluation for Ti-Mo-Zr-Ta-Si Alloys for Potential Implant Applications. *Materials* **2019**, *14*, 6806. [CrossRef]
2. Rossi, S.; Volgare, L.; Perrin-Pellegrino, C.; Chassigneux, C.; Dousset, E.; Eyraud, M. Dual Electrochemical Treatments to Improve Properties of Ti_6Al_4V Alloy. *Materials* **2020**, *13*, 2479. [CrossRef] [PubMed]
3. Zhang, L.G.; Tang, J.L.; Wang, Z.Y.; Zhou, J.Y.; Wu, D.; Liu, L.B.; Masset, P.J. Pseudo-spinodal mechanism approach to designing a near-β high-strength titanium alloy through high-throughput technique. *Rare Met.* **2020**, *40*, 2099–2108. [CrossRef]
4. Kim, K.M.; Kim, H.Y.; Miyazaki, S. Effect of Zr Content on Phase Stability, Deformation Behavior, and Young's Modulus in Ti–Nb–Zr Alloys. *Materials* **2020**, *13*, 476. [CrossRef] [PubMed]
5. Fernandes Santos, P.; Niinomi, M.; Liu, H.; Cho, K.; Nakai, M.; Trenggono, A.; Champagne, S.; Hermawan, H.; Narushima, T. Improvement of microstructure, mechanical and corrosion properties of biomedical Ti-Mn alloys by Mo addition. *Mater. Des.* **2016**, *110*, 414–424. [CrossRef]
6. Arciniegas, M.; Manero, J.M.; Espinar, E.; Llamas, J.M.; Barrera, J.M.; Gil, F.J. New Ni-free superelastic alloy for orthodontic applications. *Mater. Sci. Eng. C* **2013**, *33*, 3325–3328. [CrossRef]
7. Ibrahim, M.K.; Saud, S.N.; Hamzah, E.; Nazim, E.M. Role of Ag addition on microstructure, mechanical properties, corrosion behavior and biocompatibility of porous Ti-30 at% Ta shape memory alloys. *J. Cent. South Univ.* **2020**, *27*, 3175–3187. [CrossRef]
8. Frutos, E.; Karlík, M.; Jiménez, J.A.; Langhansová, H.; Lieskovská, J.; Polcar, T. Development of new β/α"-Ti-Nb-Zr biocompatible coating with low Young's modulus and high toughness for medical applications. *Mater. Des.* **2018**, *142*, 44–55. [CrossRef]
9. Rachinger, W. A "super-elastic" single crystal calibration bar. *Br. J. Appl. Phys.* **1958**, *9*, 250. [CrossRef]
10. Liu, S.; Liu, J.; Wang, L.; Ma, R.L.; Zhong, Y.; Lu, W.; Zhang, L.C. Superelastic behavior of in-situ eutectic-reaction manufactured high strength 3D porous NiTi-Nb scaffold. *Scr. Mater.* **2020**, *181*, 121–126. [CrossRef]
11. Ramezannejad, A.; Xu, W.; Xiao, W.; Fox, K.; Liang, D.; Qian, M. New insights into nickel-free superelastic titanium alloys for biomedical applications. *Curr. Opin. Solid State Mater. Sci.* **2019**, *23*, 100783. [CrossRef]
12. Alshammari, Y.; Yang, F.; Bolzoni, L. Mechanical properties and microstructure of Ti-Mn alloys produced via powder metallurgy for biomedical applications. *J. Mech. Behav. Biomed. Mater.* **2019**, *91*, 391–397. [CrossRef] [PubMed]
13. Li, C.; Song, Q.; Yang, X.; Wei, Y.; Hu, Q.; Liu, L.; Zhang, L. Experimental Investigation of the Phase Relations in the Fe-Zr-Y Ternary System. *Materials* **2022**, *15*, 593. [CrossRef] [PubMed]
14. Manzo-Garrido, H.; Häberle, P.; Henao, H. Experimental determination of phase equilibrium in Ti-Nb-Mn system at temperatures between 1150 °C and 1200 °C. *DYNA* **2019**, *86*, 304–311.
15. Li, C.H.; Wang, K.; Dong, H.Q.; Lu, X.G.; Ding, W.Z. Thermodynamic modeling of Ti–Cr–Mn ternary system. *Calphad* **2009**, *33*, 658–663.
16. Murray, J.L. The Mn–Ti (Manganese-Titanium) system. *Bull. Alloys Phase Diagr.* **1981**, *2*, 334–343. [CrossRef]
17. Khan, A.U.; Brož, P.; Premović, M.; Pavlů, J.; Vřeštál, J.; Yan, X.; Rogl, P. The Ti–Mn system revisited: Experimental investigation and thermodynamic modelling. *Phys. Chem. Chem. Phys.* **2016**, *18*, 23326–23339. [CrossRef]
18. Liu, S.; Hallstedt, B.; Music, D. Ab initio calculations and thermodynamic modeling for the Fe–Mn–Nb system. *Calphad* **2012**, *38*, 43–58. [CrossRef]

19. Hellawell, A. The constitution of manganese base alloys with metals of the second transition series. *J. Less Common Met.* **1959**, *1*, 343–347. [CrossRef]
20. Savitskii, E.M.; Kopetskii, C.V. Phase Diagram of the Mananese-Titanium and Manganese-Zirconium Systems. *Russ. J. Inorg. Chem.* **1960**, *5*, 1173–1179.
21. Svechnikov, V.; Petkov, V. Formation of Laves Phases in Alloys of Mn with Transition Metals of Groups IVA and VA. *Akad. Nauk Ukr. SSR Metallofiz.* **1976**, *64*, 24–28.
22. Bellen, P.; Kumar, K.H.; Wollants, P. Thermodynamic assessment of the Ni-Ti phase diagram. *Int. J. Mater. Res.* **1996**, *87*, 972–978. [CrossRef]
23. Kaltenbach, K.; Gama, S.; Pinatti, D.G.; Schulze, K.; Henig, E.T. A Contribution to the Ternary System Al-Nb-Ti, Z. *Metallkd* **1989**, *80*, 535–539.
24. Kaufman, L.; Nesor, H. Coupled phase diagrams and thermochemical data for transition metal binary systems—II. *Calphad* **1978**, *21*, 81–108. [CrossRef]
25. Kumar, C.H.; Wollants, P.; Delaey, L. Thermodynamic calculation of Nb-Ti-V phase diagram. *Calphad-Comput. Coupling Phase Diagr. Thermochem.* **1994**, *18*, 71–79. [CrossRef]
26. Zhang, Y.; Liu, H.; Jin, Z. Thermodynamic assessment of the Nb-Ti system. *Calphad* **2001**, *25*, 305–317. [CrossRef]
27. Matsumoto, S.; Tokunaga, T.; Ohtani, H. Thermodynamic analysis of the phase equilibria of the Nb–Ni–Ti system. *Mater. Trans.* **2005**, *46*, 2920–2930. [CrossRef]
28. Okamoto, H. Supplemental Literature Review of Binary Phase Diagrams: Ag-Sn, Al-Pd, Ba-Gd, Ba-Pr, Cu-P, Dy-Ni, Ga-Mn, Gd-Sb, Gd-Zr, Ho-Te, Lu-Sb, and Mn-Nb. *J. Phase Equilibria Diffus.* **2014**, *35*, 105–116. [CrossRef]
29. Liu, J.; Yang, X.; Li, C. Phase relationships in the Ho–Mn–Ti ternary system at 773 K. *J. Alloys Compd.* **2009**, *476*, 238–240. [CrossRef]
30. Okamoto, N.L.; Yuge, K.; Tanaka, K. Atomic displacement in the CrMnFeCoNi high-entropy alloy—A scaling factor to predict solid solution strengthening. *AIP Adv.* **2016**, *6*, 125008. [CrossRef]

Disclaimer/Publisher's Note: The statements, opinions and data contained in all publications are solely those of the individual author(s) and contributor(s) and not of MDPI and/or the editor(s). MDPI and/or the editor(s) disclaim responsibility for any injury to people or property resulting from any ideas, methods, instructions or products referred to in the content.